Phase transitions in the Mn-Zn fluorosilicate hexahydrates

2001 J. Phys.: Condens. Matter 13 3709

(http://iopscience.iop.org/0953-8984/13/16/302)

INSTITUTE OF PHYSICS PUBLISHING JOURNAL OF PHYSICS: CONDENSED MATTER

J. Phys.: Condens. Matter **13** (2001) 3709–3716 www.iop.org/Journals/cm PII: S0953-8984(01)17959-2

Phase transitions in the Mn–Zn fluorosilicate hexahydrates

K V Kamenev[1], **S K Asadov**[2], **V I Kamenev**[2], **I S Maksimov**[2] **and B M Todris**[2]

[1] Department of Physics and Astronomy, The University of Edinburgh, Mayfield Road, Edinburgh EH9 3JZ, UK
[2] Donetsk Physico-Technical Institute, National Academy of Sciences of Ukraine, 72 R Luxemburgh Street, Donetsk 340114, Ukraine

Received 12 October 2000, in final form 1 March 2001

Abstract

The effect of chemical substitution on the stability of structural phases in $Mn_{1-x}Zn_xSiF_6{\cdot}6H_2O$ fluorosilicate hexahydrates has been investigated by means of x-ray diffraction. Under ambient conditions the substitution of heavier Zn atoms for Mn atoms leads to a phase transition between two trigonal phases with the loss of the mirror plane symmetry. It has been found that external pressure and Zn doping have very similar effects on the phase stability of the fluorosilicate hexahydrates, and the established x–T phase diagram mirrors the generalized pressure–temperature phase diagram for the fluorosilicate hexahydrates series. The variety of the phases found and the character of the phase transitions between them are discussed in terms of a qualitative model, which takes into consideration the order–disorder processes in the material.

The fluorosilicate hexahydrates of divalent metals (M-FSH) with general formula $MSiF_6{\cdot}6H_2O$ (where M = Mn, Fe, Co, Ni and Zn) have been at the centre of attention for almost forty years as a model system for studying orientational disorder in salts [1]. The structure of M-FSH consists of rigid octahedral ions: $[M(H_2O)_6]^{2+}$ and $[SiF_6]^{2-}$. They are schematically represented in figure 1. The symmetry is rhombohedral $\bar{3}m$ with the threefold axis perpendicular to the plane of the figure. The mirror planes m include the threefold axis $\bar{3}$. They are shown by three solid lines. The large octahedron in the centre of the figure 1 is a $[M(H_2O)_6]^{2+}$ ion with oxygen atoms in the corners of the octahedron. The six smaller octahedra surrounding it represent $[SiF_6]^{2-}$ ions (two other $[SiF_6]^{2-}$ octahedra above and below the central octahedron are not shown for clarity). The anion and the cation are connected by hydrogen bonds shown as dotted lines.

Comparison of the results obtained from diffraction [2–5] and NMR [6–8] studies shows that the phases found in the various M-FSH differ not only in the elements of symmetry present in the structure, but also in the dynamics of the $[M(H_2O)_6]^{2+}$ and $[SiF_6]^{2-}$ ions. The structural disorder observed in the M-FSH series manifests itself in the presence of two possible positions for each type of ion. These positions are shown by small circles labelled as (A) and (B) for

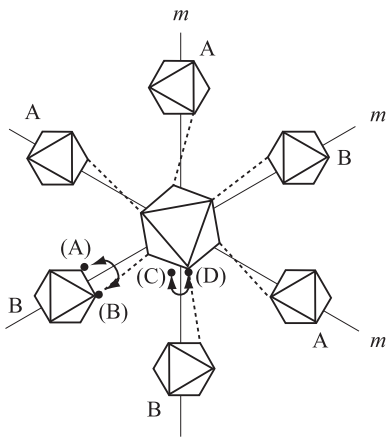

Figure 1. A schematic representation of the orientational disorder in the structure of M-FSH. The large octahedron is a $[M(H_2O)_6]^{2+}$ ion and the six smaller octahedra are $[SiF_6]^{2-}$ ions. The threefold axis $\bar{3}$ is perpendicular to the plane of the figure and is included in the mirror planes m, shown as solid lines. The dotted lines represent the hydrogen bonds. Small filled circles labelled (A), (B), (C) and (D) show the two possible positions for $[SiF_6]^{2-}$ and $[M(H_2O)_6]^{2+}$ ions. The arrows show the directions of librations of the octahedra.

$[SiF_6]^{2-}$ and as (C) and (D) for $[M(H_2O)_6]^{2+}$ ions. The position of each octahedron can then be defined according to the position of its bonded corner ((D) for the $[M(H_2O)_6]^{2+}$ ion in figure 1). The mirror plane m relates the position (A) to (B) and the position (C) to (D). In the case of dynamic disorder for both types of ionic complex, the octahedra librate between the two possible positions for each ion. At any given time the anions and cations are equally distributed over the two possible positions. This gives the average structure with the mirror symmetry element m and the symmetry of either the $R\bar{3}m$ or $P\bar{3}m1$ space group, observed in Mn- and Fe-FSH. The $[M(H_2O)_6]^{2+}$ complexes are generally larger than the $[SiF_6]^{2-}$ ions. As the ionic radius of the constituting metal M increases, the reorientation motion of the $[M(H_2O)_6]^{2+}$ octahedra stops, creating static disorder [8]. When this happens, the distribution of the metal–water complexes between the positions (C) and (D) is not equal over the crystal. This leads to the loss of the mirror plane m, and the structural symmetry is reduced to $R\bar{3}$. This phase is observed under ambient conditions in Co-, Ni- and Zn-FSH. It is called the $\alpha(R\bar{3})$ phase to distinguish the structure from that in the case of total static structural disorder, when both $[M(H_2O)_6]^{2+}$ and $[SiF_6]^{2-}$ octahedral complexes cease their reorientation motion—the $\beta(R\bar{3})$ phase. The fully ordered phase has a monoclinic symmetry: $P2_1/c$.

Studies of the influence of hydrostatic pressure on the stability of the crystallographic states in the M-FSH have shown that these materials obey the homological rule [9]. This is demonstrated by the generalized pressure–temperature (P–T) phase diagram presented in figure 2. The various phases in this diagram are labelled according to their symmetry groups. The regions of existence of each of the phases are shown by the different types of hatching. The areas marked with the cross-hatching are those in which the metastable states can be realized due to the hysteresis along the temperature or pressure axis. The P–T phase diagram for each member of the M-FSH series can be presented as a part of the generalized phase diagram extending to the right from the vertical line, corresponding to the particular M-FSH.

The generalized P–T phase diagram is the manifestation of the following property of the M-FSH series: increased atomic number is equivalent to increased pressure. For example, at ambient pressure Co-FSH exhibits structural phases and phase transitions which for Fe-HFS or

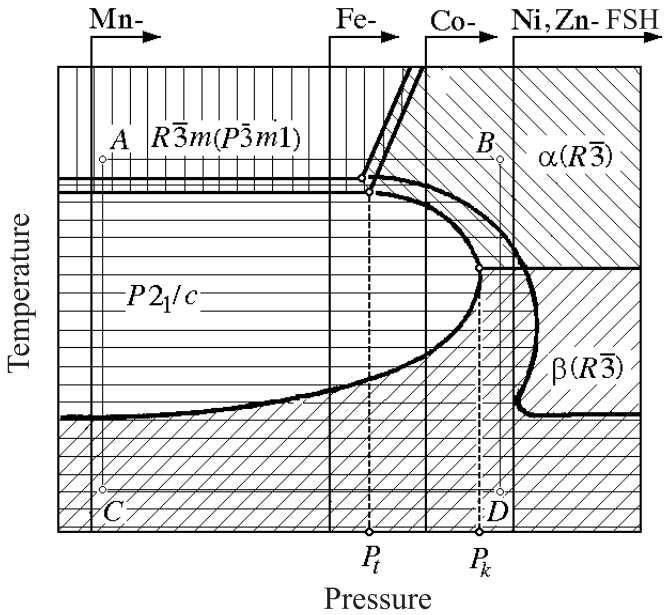

Figure 2. The generalized P–T phase diagram of the crystalline phases of the fluorosilicate hexahydrates of 3d metals.

Mn-FSH can only be achieved at high pressures. The end members of the series are Mn-FSH and Zn-FSH. From figure 2 it can be assumed that the phase behaviour of Mn-FSH can be 'transformed' into the phase behaviour of Zn-FSH by continuous substitution of lighter metals for the heavier metal atoms just as it can be done by applying external pressure. In this paper we report on the effect of the substitution of Zn for Mn atoms on the phase behaviour of the $Mn_{1-x}Zn_xSiF_6{\cdot}6H_2O$ compound ((Mn, Zn)-FSH).

The single crystals of $Mn_{1-x}Zn_xSiF_6{\cdot}6H_2O$ with $x = 0$, 0.02, 0.10, 0.25, 0.50, 0.75, 1.00 were grown from aqueous solutions [10]. The studies were carried out by means of x-ray diffraction on a diffractometer using a cryostat. The high-pressure cell made in the form of a beryllium–copper cylinder was connected to a gas compressor by a steel capillary. Due to the technical difficulties, the cryostat with the pressure cell inside could not be tilted much from the vertical axis to access more reflections, which would have allowed us to perform a full analysis of the structural symmetry. The starting point for identification of the high-pressure phases was the generalized pressure–temperature phase diagram of crystal structures presented in figure 2. The phase boundaries were identified by the anomalies in the dependencies on the Zn doping and temperature of the lattice parameters, the intensity and the shape of the selected reflections. Single crystals were aligned and mounted on the sample holder inside the pressure cell in such a way that the selected characteristic reflections could be observed during the measurements. The temperature variations were performed in the temperature interval between 79 K and 320 K. The temperature was stabilized and measured with the accuracies of ± 0.5 K and ± 0.3 K, respectively. The x-ray diffraction studies were performed by the Bragg–Brentano method. The lattice parameters were calculated from the positions of the (10 0 0) planes using Ni Kα radiation ($2\theta \approx 123^\circ$) and from the positions of the (12 0 0) planes using Ni Kβ radiation ($2\theta \approx 134^\circ$). The accuracies of the determinations of the lattice parameters were $\pm 0.1\%$ and $\pm 0.01\%$, respectively. The phase transition between the states with the

trigonal and monoclinic symmetries of the crystal lattice was indicated by a sharp deformation of the (10 0 0) peak profile, which was due to the appearance of the domain structure at the transition into the lower-symmetry phase. This deformation is described in [11].

In figure 3 we present the dependences of the lattice parameters a_h and c_h along hexagonal axes on the Zn doping level at room temperature. For comparison, in figure 4 we show the lattice parameters a_h and c_h along the same hexagonal axes for the M-FSH series and indicate the symmetry groups. The transition from the $R\bar{3}m$ or $P\bar{3}m1$ symmetry of the M-FSH members (Mn-FSH) to the space group $\alpha(R\bar{3})$ (Zn-FSH) is accompanied by a sharp decrease in the lattice parameter a_h (figure 4). A similar drop is observed in the (Mn, Zn)-FSH series between the doping levels of $x = 0.02$ and $x = 0.10$ (figure 3). This allows us to conclude that the samples with $x < 0.02$ crystallize with the $P\bar{3}m1$ symmetry space group, and those with $x > 0.1$ with the $\alpha(R\bar{3})$ symmetry group. We would like to note here that the transition between these two

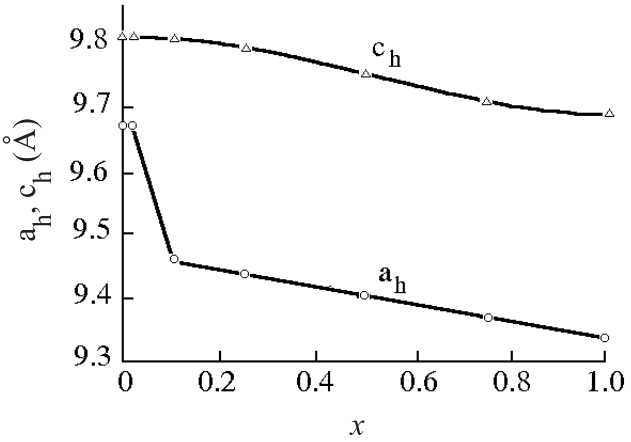

Figure 3. The dependences of the lattice parameters a_h and c_h on the Zn doping level in the series $Mn_{1-x}Zn_xSiF_6{\cdot}6H_2O$.

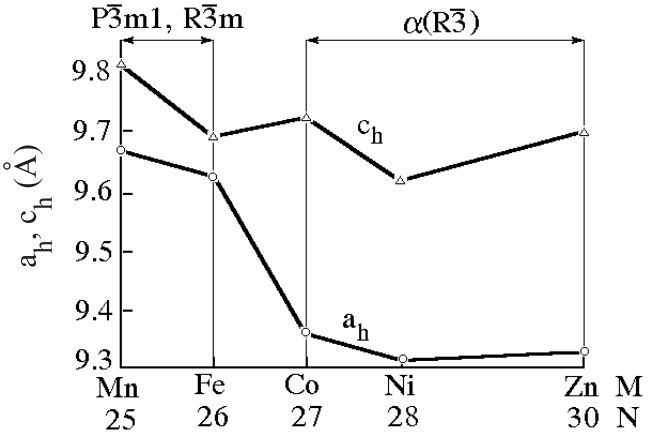

Figure 4. The lattice parameters a_h and c_h under ambient conditions and the corresponding symmetry groups for the various M-FSH as functions of the atomic number of the constituting metal M.

symmetry groups with doping is homogeneous, i.e. all of the samples of the (Mn, Zn)-FSH series were found to be of a single phase.

The temperature dependencies of the a_h-parameter for various values of x obtained during the descending temperature variations are presented in figure 5. The (10 0 0) diffraction peak, which was used in this study to define the $a_h(T)$ dependence, was only present for the compositions with $x < 0.25$ above the temperature $T_{s\uparrow}$. Below this temperature the peak disappears, and we observe reflections characteristic of the $P2_1/c$ symmetry group [11]. In other words, the samples of the (Mn, Zn)-FSH series with $x < 0.25$ experience a phase transition into the monoclinic crystal lattice. This phase transition is of first order since the group $P2_1/c$ is not a subgroup of $P\bar{3}m1$. In figure 6 we present the temperature dependence of the (10 0 0) integrated intensity $I_{(10\,0\,0)}$ obtained during both cooling and heating. A pronounced hysteresis is observed for all of the samples with $x < 0.25$, clearly showing the first-order nature of the phase transition.

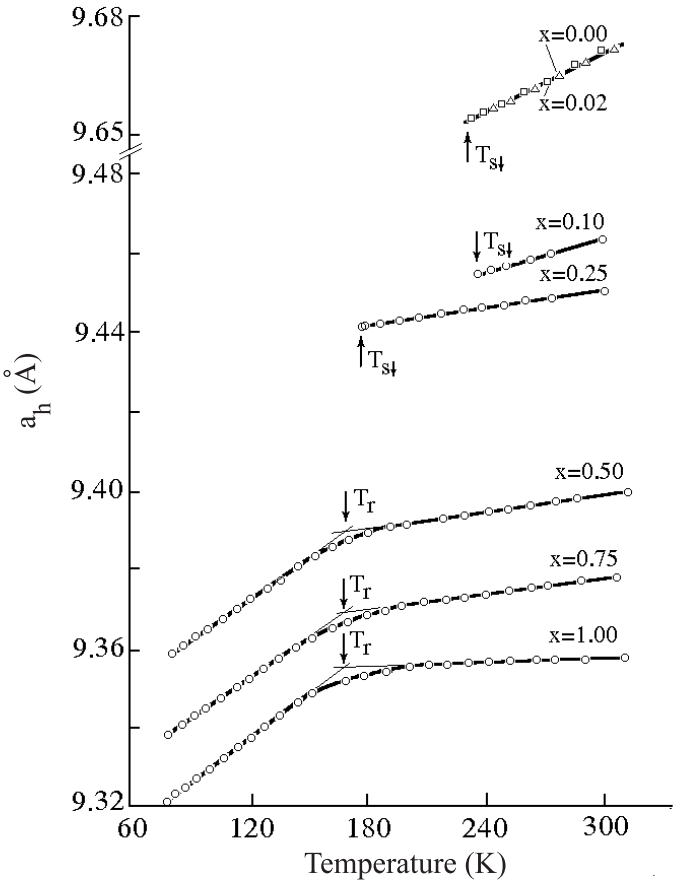

Figure 5. The temperature dependence of the lattice parameter a_h for members of the (Mn, Zn)-FSH series with various levels of Zn doping.

For compositions with $x > 0.50$ the (10 0 0) peak is present over the entire temperature region studied (figure 5). The change in the slope of $a_h(T)$ at $T = T_r$ is characteristic of the $\alpha(R\bar{3}) \Leftrightarrow \beta(R\bar{3})$ second-order phase transition [12–14].

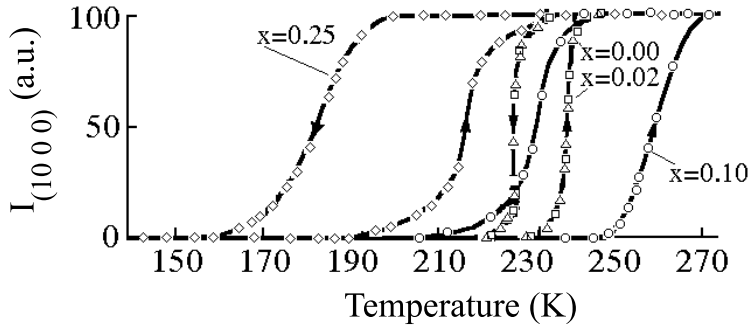

Figure 6. Temperature dependencies of the integrated intensity of the (10 0 0) reflection near the phase transition into the low-temperature monoclinic phase for several members of the $Mn_{1-x}Zn_xSiF_6{\cdot}6H_2O$ series. Arrows are used to indicate ascending and descending temperature variations.

The results described above are summarized in the x–T phase diagram (figure 7). Comparison of the x–T phase diagram and the generalized P–T phase diagram (figure 2) shows their qualitative agreement. According to the differences in phase behaviour, the (Mn, Zn)-FSH series can be divided into three types.

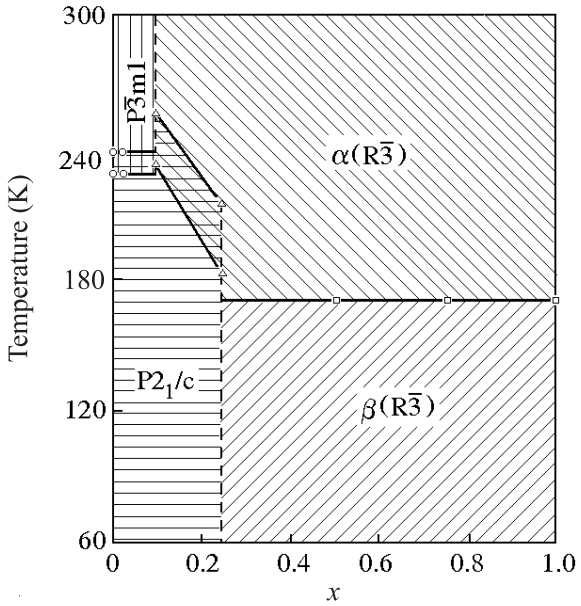

Figure 7. The x–T phase diagram of the $Mn_{1-x}Zn_xSiF_6{\cdot}6H_2O$ series.

The first group of samples with $x = 0, 0.02$ at room temperature possess the trigonal crystal lattice with the space group $P\bar{3}m1$. On cooling, the members of this group undergo a first-order structural phase transition into the monoclinic $P2_1/c$ phase. The analogues to this group of (Mn, Zn)-FSH are Mn-FHS and Fe-FHS. Similar phase behaviour is also observed for Mn-FHS and Fe-FHS at pressures below the triple point P_t on the generalized P–T phase diagram (figure 2).

The second group of (Mn, Zn)-FSH consists of the samples with $x = 0.25$ and 0.50. At room temperature they possess trigonal symmetry $\alpha(R\bar{3})$. Just like the members of the first group, they undergo a phase transition into the $P2_1/c$ phase on cooling. The material corresponding to this group in the M-FSH series is Co-FSH. Similar behaviour is also characteristic of any M-FSH with M = Mn, Fe or Co in the pressure region between P_t and P_k (figure 2).

Finally, the third group of (Mn, Zn)-FSH is formed by the compounds with high Zn doping level ($x = 0.50$, 0.75 and 1.00). Like the members of the second group, they crystallize into the $\alpha(R\bar{3})$ lattice under ambient conditions. However, the $R\bar{3}$ symmetry remains stable when the temperature is lowered. The change in the slope of the $a_h(T)$ dependence (figure 5) indicates the $\alpha(R\bar{3}) \Rightarrow \beta(R\bar{3})$ phase transition. Similar behaviour can be found for Ni-FSH and Zn-FSH, and also for other M-FSH at pressures higher than P_k (figure 2).

The mutual orientations of the octahedra (and consequently, the phase diagram of a M-FSH) depend on the height of the potential barrier separating the two possible orientations of the octahedra, on the energy of their thermally activated librations and on the energy gain when they undergo a phase transition into the ordered monoclinic phase. The height of the potential barrier separating the two possible orientations of the octahedra is determined by the competition of the three types of bonding in the crystal: (i) the ionic bond, creating the overall attractive force between $[M(H_2O)_6]^{2+}$ and $[SiF_6]^{2-}$ octahedra, (ii) the repulsive forces between F and O ions in the corners of the octahedra and (iii) the hydrogen bonds between F and O atoms. The repulsive forces between F and O result in the buckling of the O–H–F linkages and in the deviation of the F and O atoms from the mirror planes (figure 1) in an attempt to increase the F–O separation distance. Externally applied pressure shortens the distance between the $[M(H_2O)_6]^{2+}$ and $[SiF_6]^{2-}$ octahedra. So does the increase in the atomic number of the metal (figure 3, figure 4). With the octahedra closing in, the repulsive forces and, consequently, the height of the potential barrier increase. This can be understood even from considering the stacking of the octahedra (figure 1)—the closer the octahedra, the more difficult the rotation between positions A and B and also C and D is. It has also been found that the decrease of the distance between the octahedra results in increase of the O–F distance [2, 3].

Taking into account all of the above, we can picture the phase behaviour of the M-FSH series in the following way. At room temperature and relatively low pressures, in the M-FSH with small atomic number of M the octahedra have enough thermal energy to overcome the potential barrier, separating their orientational positions. Under these conditions the octahedra librate and the crystal symmetry includes the $\bar{3}m$ element. When the temperature is lowered, the crystal undergoes a transition into a more favourable ordered state with the symmetry $P2_1/c$. Increased atomic number of the metal or increased applied pressure raises the potential barrier. As a consequence, the $[M(H_2O)_6]^{2+}$ octahedra become statically disordered at room temperature. The symmetry of the crystal is lowered to $\alpha(R\bar{3})$. The cooling of the crystal first leads to the phase transition into the ordered $P2_1/c$ monoclinic phase, being the most favourable state for the lattice. However, such a transition (requiring the ordering of the disordered octahedra) is complicated by the necessity to overcome the potential barrier separating the two possible orientations. Therefore, an inverse dependence of the temperature of the $\alpha(R\bar{3}) \Leftrightarrow P2_1/c$ phase transition on the applied pressure (the region between P_t and P_k in figure 1) or on the doping level of the heavier metal atoms (the region between $x = 0.10$ and $x = 0.25$ in figure 6) is characteristic for this group of M-FSH. When the applied pressure or the atomic number of M ($x > 0.25$ in figure 6) is increased even further, the potential barrier becomes too high to be overcome. Therefore, at lower temperatures, the crystal undergoes the $\alpha(R\bar{3}) \Rightarrow \beta(R\bar{3})$ phase transition due to the change in the disorder type for $[SiF_6]^{2-}$ octahedra from dynamic to static.

In conclusion, we have studied the effect of Zn doping on the structural phases of $Mn_{1-x}Zn_xSiF_6{\cdot}6H_2O$ single crystals and have summarized the results in an x–T phase diagram. The comparative analysis of the x–T phase diagram of the (Mn, Zn)-FSH and the generalized P–T phase diagram for the M-FSH series has shown that the application of the external pressure and the increase in the atomic number of the metal M have a similar effect on the members of the M-FSH series. The proposed mechanism for the pressure- or doping-driven phase transitions, despite its simplicity, can explain not only the general rules for the behaviour of M-FSH, but also some unique features found in the salts of this series. Similar ideas can be applied to a wider range of materials with hydrogen bonds, exhibiting order–disorder or static–dynamic disorder transitions.

Acknowledgments

The authors acknowledge very useful discussions with G J Ackland. KVK thanks the Royal Society (London) for the travel grant 22397/994/A2B.

References

[1] Parsonage N G and Staveley L A K 1978 *Disorder in Crystals* (Oxford: Clarendon)
[2] Hamilton W C 1962 *Acta Crystallogr.* **15** 353
[3] Ray S, Zalkin A and Templeton D 1973 *Acta Crystallogr.* B **29** 2741
[4] Kodera E *et al* 1972 *J. Phys. Soc. Japan* **32** 863
[5] Sysoyama S and Osaka K 1972 *Acta Crystallogr.* B **28** 2626
[6] Rangarajan G and Ramakrishna J 1969 *J. Chem. Phys.* **51** 5290
[7] Muthukrishnan K and Ramakrishna J 1973 *J. Chem. Phys.* **59** 557
[8] Skjaeveland S M and Svare I 1974 *Phys. Scr.* **10** 273
[9] Asadov S K *et al* 1993 *Fiz. Tekh. Vys. Davl.* **3** 21
[10] Kabanova N G *et al* 1978 *Kristallografiya* **6** 1235
[11] Chevrier P, Hardy A and Jehanno G 1981 *Acta Crystallogr.* A **37** 578
[12] Asadov S K *et al* 1992 *Fiz. Tekh. Vys. Davl.* **2** 104
[13] Asadov S K *et al* 1991 *Ukr. Phys. J.* **36** 293
[14] Asadov S K *et al* 1997 *J. Phys.: Condens. Matter* **9** 7161